Geimer Paul (Orcid ID: 0000-0003-2627-5507)

Finnegan Riley (Orcid ID: 0000-0003-3234-6439)

Moore Jeffrey, R (Orcid ID: 0000-0001-5831-2048)

Sparse Ambient Resonance Measurements Reveal Dynamic Properties of Freestanding Rock Arches

Paul R. Geimer[1], Riley Finnegan[1], Jeffrey R. Moore[1]

[1]Department of Geology & Geophysics, University of Utah

Corresponding author: Paul Geimer (paul.geimer@utah.edu)

Key points:

- Single-station ambient vibration data and numerical modeling describe the dynamic response of natural arches with limited site access
- Dense seismic array directly resolves resonant mode shapes, validating predictions of simple bending modes and fixed boundary conditions
- Sandstone arches in Utah resonate between 1-40 Hz, exhibit low damping, and have stiffness that vary with diagenetic conditions

This article has been accepted for publication and undergone full peer review but has not been through the copyediting, typesetting, pagination and proofreading process which may lead to differences between this version and the Version of Record. Please cite this article as doi: 10.1029/2020GL087239

Abstract

The dynamic properties of freestanding rock landforms are a function of fundamental material and mechanical parameters, facilitating non-invasive vibration-based structural assessment. Characterization of resonant frequencies, mode shapes, and damping ratios, however, can be challenging at culturally-sensitive geologic features, such as rock arches, where physical access is limited. Using sparse ambient vibration measurements, we describe three resonant modes between 1 – 40 Hz for 17 natural arches in Utah spanning a range of lengths from 3 – 88 m. Modal polarization data are evaluated to combine field observations with 3-D numerical models. We find outcrop-scale elastic moduli vary from 0.8 to 8.0 GPa, correlated with diagenetic processes, and identify low damping at all sites. Correlation of dense-array measurements from one arch validate predictions of simple bending modes and fixed boundary conditions. Our results establish use of sparse ambient resonance measurements for structural assessment and monitoring of arches and similar freestanding geologic features worldwide.

Plain Language Summary

Natural rock arches vibrate under ambient conditions with a unique set of frequencies controlled by geometry, host material, and interactions with nearby bedrock. Recent rockfall events at well-known arches in Utah have highlighted the need to develop non-invasive assessment methods to better understand how these sensitive landforms evolve. To reduce site impacts, we employed limited instrumentation to measure ambient vibrations of 17 arches across Utah for identification of resonant frequencies. We combine direct observations with predictive numerical models to visualize resonant mode shapes and describe the controlling material properties and structural boundaries. In defining the first three modes of each site, we are able to characterize dynamic properties at arches encompassing several geologic formations and a range of length scales. These results establish a versatile method for structural evaluations of arches and other significant freestanding geologic features.

1 Introduction

Ambient vibrations of manmade and natural structures are stimulated by broadband excitation sources such as wind, anthropogenic activity, and seismicity. The resulting induced resonant modes are a function of primary structural and material properties, notably boundary conditions, damping, density, and elastic modulus (Ewins, 1984). Non-invasive monitoring of modal characteristics has thus been broadly employed to monitor changes within the built environment, with structural health monitoring (SHM) techniques used extensively in civil engineering for characterization of recoverable and permanent mechanical changes (Doebling et al., 1996).

SHM studies often employ induced resonance, allowing for limited instrumentation to assess both sudden and progressive structural changes (Peeters & De Roeck, 2001). Applications range from early work on evolving resonant modes of a bridge during ongoing construction (Carder, 1937) to influences of water level on an artificial dam (Darbre et al., 2000). In studies of seismic hazards, SHM has shown value in assessing the impact of earthquakes on buildings (Michel & Gueguen, 2010); e.g. Clinton et al. (2006) traced more than 75% of the long-term frequency drop of the Caltech Millikan Library to a single earthquake.

While development and application of SHM methods have historically focused on engineered structures, there is a growing body of research applying time-dependent modal analysis to geologic features (Larose et al., 2015). Ambient vibration measurements and numerical

modeling have been used to assess the dynamics of unstable rock columns and landslides (Lévy et al., 2010; Bottelin et al., 2013a; Bottelin et al., 2013b; Kleinbrod et al., 2017) while human activities, including explosions, machinery, and artificial reservoirs, have been analyzed for their impacts on rock landforms with high cultural value (Dowding & Cummings, 1983; King & Demarco, 2003; Moore et al., 2016). SHM of natural rock arches is in turn motivated by rockfall events at Landscape Arch in 1991 and 1995, and the collapse of nearby Wall Arch (both in Arches National Park) in 2008. Studies to date, however, have been narrow in scope, with single-site evaluations of dynamic properties (Moore et al., 2016; Starr et al., 2015) and assessment of stiffness variations within a single geologic unit (Moore et al., 2018).

In this study, we apply ambient vibration modal analysis from sparse seismic arrays to a varied collection of natural rock arches. We compare quantitative assessments of sites across different scales and host lithologies to facilitate more complete understanding of the strengths and limitations of the technique, as well as provide detailed characterization of mechanical and structural variations in these iconic desert landforms. Our results establish the methodology and highlight its limitations, permitting broad application to similar freestanding geologic features worldwide.

2 Study Sites

The 18 natural arches in this study are located in the Colorado Plateau of southern Utah (Figure 1, Table 1), with 17 sites measured using sparse sensor deployments and 1 site characterized with a dense seismic array. Arch spans vary from 3 to 88 m, including the longest arch in North America (Landscape Arch). In addition to access considerations, sites were selected for simple and slender geometries facilitating interpretation of limited ambient vibration data and construction of 3-D photogrammetric models. One site (Rainbow Arch) collapsed during the winter of 2018-19, after the completion of field measurements.

The majority of arches analyzed are hosted in Jurassic sandstones (Table 1), with the greatest number of sites in the cross-bedded Navajo Sandstone, and others formed from the interbedded Kayenta Formation, massive cliffs of the Wingate Sandstone, or smooth exposures of the Entrada Sandstone (Doelling, 2004). Other materials in this study include calcareous sandstone of the Paleogene Claron Formation (Biek et al., 2015), Permian cross-bedded White Rim Sandstone, thickly cross-bedded Cedar Mesa Sandstone, and interbedded sandstone of the Lower Cutler Group (Doelling, 2004).

3 Methods

3.1 Sparse Ambient Vibration Measurements

We recorded ambient vibrations of rock arches using temporary seismometer installations. Limited or restricted site access led to standardization of a sparse, two-station deployment at each site, arranged in an active-reference configuration. We used three-component broadband Nanometrics Trillium Compact 20s seismometers and 24-bit Centaur data loggers recording at 100-200 Hz, varying with arch size. Each active station was placed on the arch lintel, with reference stations installed 50-200 m away on flat bedrock. Instruments were set on intact rock surfaces, leveled and aligned to magnetic north, and shielded from wind and temperature variations. Measurement details are given in Figure S1 and Table S1.

Ambient vibration data were analyzed for modal properties of each arch, including frequency content, mode shapes, and damping ratios. We first removed the mean, trend, and instrument

response from all channels. Horizontal channels were rotated to longitudinal (parallel) and transverse (perpendicular) of the arch orientation. We calculated the power spectral density (PSD) of each component for one-hour records following McNamara & Buland (2004). Each PSD was estimated using Welch's method, with stacked fast Fourier transforms of 40.96 s Hanning-tapered windows, 50% overlap to reduce variance, and smoothing over a 0.12 Hz window (Welch, 1967). Modal peaks resulting from arch resonance were distinguished from instrumental noise and undesired local sources by narrow spectral peaks and high spectral ratios with reference stations. As the number of identifiable modes varied at each site due to excitation levels and active station location, our analysis focused on the first three modes, which could be reliably detected across the sites. Viscous damping ratios of fundamental modes were estimated with the half-power width of the PSD peak, averaging results over 10 time windows Hanning-tapered by 5% and overlapping by 10%. For several smaller arches, we verified damping using the logarithmic decay of manual impulses (Silva, 1999).

Using polarization analysis described by Park et al. (1987) and modified by Koper & Hawley (2010), we constrained mode shapes by characterizing particle motion at the active station. Eigen-decomposition was applied to the spectral covariance matrix to obtain frequency-dependent polarization attributes of incidence and azimuth, as well as nondimensional degree of polarization to coherence of the motion. Similar to the PSD workflow, we applied eigen-decomposition over short overlapping time windows, generating probability distributions to constrain mode shape parameters (Figures S2-18).

3.2 Numerical Modeling

We used finite element analysis (FEA) to visualize resonant mode shapes and constrain the structural and material properties required to replicate modal behavior at the active station location. Implementation of FEA first required construction of accurate 3-D geometries for each arch. We generated georeferenced ground- and drone-based images and aligned photosets using commercial structure-from-motion photogrammetry software (Bentley Context Capture: www.bentley.com) to create 3-D surface models, with scaling verified by field measurements. Model refinement was performed in Meshmixer (www.meshmixer.com), e.g. filling holes from incomplete photo coverage, smoothing irregular surfaces, and transforming the surface into a solid 3-D object. We relied on field assessments to crop the final model, removing distal material not participating in the resonant modes.

We used the FEA software COMSOL Multiphysics (www.comsol.com) to perform eigenfrequency analyses of the 17 photogrammetry-derived 3D arch models. Homogenous material properties were assigned based on the largely massive and unfractured texture of the host sandstones, as well as confinement of individual arches to single stratigraphic units. We applied fixed boundaries to replicate confined in-situ conditions. Forward modeling resulted in estimates of material properties able to reproduce the first three observed resonant frequencies at each site. Under assumptions of linear elasticity, small deflections, and consistent boundary conditions, the resonant frequencies (f_i) of a beam vary as:

$$f_i \propto \sqrt{\frac{E}{\rho}}$$

Where E is the Young's modulus and ρ density (Chopra, 2011). Following data collected from representative Navajo and Wingate sandstone samples in southern Utah, we held

density constant at 2000 kg/m^3 for all materials and allowed *E* to vary to reproduce observed resonant frequencies (Moore et al., 2018).

Polarization agreement between numerical results and field data was evaluated by extracting predicted particle motion vectors for the simulated eigenmodes at active station locations. For each arch, we assessed the resulting agreement with a normalized misfit function based on the resonant frequency and vector orientation of the first three modes (Table 1; Text S1,S2). This metric allowed for qualitative comparison of modal analysis success across all study sites. Misfit was used to guide changes to forward modeling – via adjustments to boundary conditions, geometry, or modulus – and improve the overall agreement.

3.3 Dense geophone array correlation

At Musselman Arch in Canyonlands National Park, the 37-m-long, beam-like span facilitated a deployment of a dense array to identify mode shapes in-situ. While insufficient 3-D modeling of surrounding material prevented comparison to FEA results, we designed the array to validate assumptions regarding modal behavior and boundary conditions. We deployed 30 three-component Fairfield Zland 5 Hz nodal geophones across the arch for 125 minutes in December 2017, sampling at 250 Hz. The array consisted of two parallel lines 1 m apart with 5 m station spacing (Figure 2).

We calculated normalized correlation coefficients across the array to identify mode shapes, extracting the stable amplitude and phase differences between stations during resonance (Farrar & James III, 1997). Data were first downsampled to 50 Hz and rotated to the arch reference frame. We cut data into five-minute detrended, tapered windows without overlap. Following Bensen et al. (2007) and Lin et al. (2013), we applied spectral whitening prior to cross-correlation of all station combinations in each line. We used the maximum window amplitudes for temporal normalization, prior to stacking each station-pair correlation to generate nine cross-correlograms (ZZ, ZT, ZL, etc.). Analogous to the correlation coefficient but avoiding re-correlation for each passband, we filtered cross-correlograms to frequency peaks on individual PSDs and extracted the zero-time lag amplitude for each station-pair, omitting noisy auto-correlation amplitudes, creating a curve for each station in the line. Curves with a root-mean-square (RMS) within the largest 75% for each line were normalized by the RMS and averaged to calculate the final normalized correlation amplitude curve and error (Figure 2).

4 Results

4.1 Ambient vibration modal analysis

We identified and characterized the first three resonant modes of 17 arches (Figure 3a), with misfit quantified between observed and predicted results (Table 1). The majority of modes are simple vertical or transverse bending modes. Second-order bending is also well-resolved when present among the first three modes. Torsional bending is less common, primarily occurring at sites with pronounced geometric asymmetry and small fixed boundaries relative to arch span, e.g. Sunset Arch or Arsenic Arch.

Application of the cumulative misfit function to the full dataset reveals Moonshine Arch to be the best match, with strong model agreement facilitated by clear geometry and boundary conditions, as well as active station placement near the center of the span, optimal for

accurately capturing low-order bending modes (Figure 4). This stands in contrast to the similarly clear Corona Arch, where the second and third modes were poorly captured at the active station location, resulting in a large relative misfit (Table 1).

We find the combination of single-station vibration measurements and numerical modeling is sufficient to constrain outcrop-scale stiffness and damping values. Despite modeling uncertainties related to boundary conditions, instrument placement, and material heterogeneity, estimated elastic moduli cluster within an order of magnitude across seven geologic formations, ranging from 0.8 to 8.0 GPa with 65% of sites between 2 and 5 GPa (Figure 3b). The Navajo Sandstone, hosting the largest number of sites (9), exhibits moduli ranging from 0.8 to 4.7 GPa. We find damping to be consistently low (< 4%), measured with half-power width and verified by logarithmic decay of impulsive excitations (Table 1). This is consistent with high spectral amplification observed between the active and reference stations (Chopra, 2011).

4.2 Musselman Arch mode shapes

Normalized correlation amplitudes across the Musselman Arch dense array captured five bending modes below 10 Hz (first three modes shown in Figure 2), with mode shape orientation extracted from the relative amplitudes of channel combinations (i.e. strongest correlation on ZZ suggests vertical bending). Phase shifts reveal higher-order bending modes, illustrating how single-station observations can be adversely affected by node point locations (Figure 2f). Comparison between the parallel array lines produced highly similar and well-constrained shapes for each of the first three modes. The 5-Hz geophone corner frequency does not impact results under ambient excitation, with similarly stable mode shapes extracted above and below the corner (cf. Ward & Lin, 2017).

5 Discussion

Characterization of the first three resonant modes of arches provides a standard for evaluation of a diverse and multi-scale collection of sites. With the majority of sites similarly fixed by adjacent bedrock abutments, arch span generally correlates with resonant frequency. However, several sites – notably Rainbow Bridge, Causeway Arch, and Arsenic Arch – have lower resonant frequencies than predicted by span alone (Figure 3). This is a function of a more freestanding geometry causing vibrational behavior closer to that of a cantilever, lowering resonant frequencies and demonstrating the added value of FEA modeling to validate irregular modal geometries (Young & Budynas, 2002). Large relative misfit between observed and predicted results is a function of suboptimal observation locations (e.g. measurement at a node point) and poorly constrained boundary conditions – often caused by inaccessible or obscured bounding fractures. Misfit due to material heterogeneities appears to be present at several sites (Moonrise Arch, Rainbow Arch, Squint Arch), with possible anisotropy-driven split modes observed in PSDs not reproduced by our model results (Zadler et al., 2004).

Direct mode-shape observations from the Musselman Arch array validate the sparse modal analysis method applied to other arches. Characteristically low correlation amplitudes off the lintel for all resonant modes indicate simple bending involves minimal contributions from adjacent bedrock abutments. This suggests spatially-compact 3-D models with artificially fixed boundary conditions reflect real-world behavior and are sufficient to simulate realistic

mode shapes (Moore et al., 2016). Similarly, smooth variations in amplification and phase support inclusion of homogenous materials in forward modeling.

Modeled elastic moduli reflect outcrop-scale stiffness, which is not easily assessed in-situ by other means (Hoek & Diederichs, 2006). Published empirical relations often scale the behavior of lab-tested cores to account for decreased stiffness resulting from inclusion of discontinuities such as bedding and joints (Bieniawski, 1978). With stiffness of Navajo and Wingate sandstone samples between 10 and 15 GPa (Moore et al., 2018), and all arch moduli values falling below this range, our synthesis of observed and modeled resonance appears able to incorporate outcrop-scale heterogeneities to produce reasonable moduli estimates.

Our results indicate that sparse-array modal analysis is sensitive to the effects of diagenetic alteration on outcrop-scale elastic moduli, distinguishing these effects from variations in estimated methodological quantities like boundary conditions and material heterogeneity. Limited impact of these systematic uncertainties is supported by comparison of Corona Arch and Longbow Arch (located 4 km apart), which have distinct geometries and boundary conditions but share a stratigraphic setting, resulting in nearly identical moduli estimates. While we find elastic moduli to be similar across host formations, systematic material variations may explain notable outliers and trends (Figure 3b). Several of the highest moduli are associated with the longest arches in the study (e.g. Landscape Arch, Owachomo Bridge, Rainbow Bridge), suggesting that increased stiffness of the host rock contributes to the formation of large spans, independent of underlying tectonic or geomorphic factors. Consistently low damping across the study sites further supports the idea that natural arches behave similarly to engineered structures and can be modeled with the same FEA tools to predict dynamic behavior (Satake et al., 2003).

Conversely, arches with low elastic moduli may reflect diagenetic effects related to stratigraphic position (Moore et al., 2018). Aqueduct Arch, in the iron-depleted upper Wingate, has an elastic modulus lower than the average of the similar eolian Navajo sandstone. Likewise, Moonshine and Squint Arches share a bleached appearance and below-average elastic modulus, reflecting grain-rind degradation due to iron removal by reducing fluids along flanks of Laramide uplifts (Beitler et al., 2005; Loope et al., 2010). Among unbleached sites, Arsenic Arch and Causeway Arch show evidence for recent rockfall and significant weathering along cross-bedding, suggesting anomalously low stiffnesses are associated with weak or leached cements. Tectonic factors may also play a role in softening the host rock, with Rainbow Arch formerly located within shattered strata adjacent to the Moab fault (Doelling et al., 2002).

6 Conclusion

We have established sparse ambient vibration measurements as a robust and adaptable non-invasive tool for assessing the dynamic properties of rock arches, which share limited access and cultural prominence with similarly freestanding geologic features worldwide. We combined single-station seismic data with 3D numerical modeling to characterize the modal properties of 17 arches in southern Utah. Low damping ratios produced high spectral amplifications that allowed for at least three resonant modes between 1 and 40 Hz to be characterized under ambient excitation. Methods to assess boundary conditions and mode shapes produced consistent agreement in features over a range of scales. Results of our predictive modeling were supported by correlation of a dense array across Musselman Arch, demonstrating ambient excitation of simple resonant mode shapes with fixed boundary conditions. We find elastic modulus varies systematically with diagenetic alteration across

multiple geologic units. Results from this study demonstrate key dynamic properties of rock arches and similar freestanding landforms can be deduced using a versatile workflow that combines polarization of sparse ambient vibration data with photogrammetry-based 3D numerical models.

Acknowledgements and Data

This study was funded by National Science Foundation grant EAR-1424896. We thank the University of Utah Center for High Performance Computing, Michael Thorne, Keith Koper, and Elizabeth Berg for access and implementation of computational resources. We also thank two anonymous reviewers and the associate editor for valuable feedback. Site access was provided by Arches, Bryce Canyon, and Canyonlands National Parks; and Natural Bridges and Rainbow Bridge National Monuments. Ben White, Jackson Bodkter, Ashley Russon, Ammon Hatch, Cynthia Gardner, Kathryn Vollinger, and Natan Richman helped with field work. Data generated by this study are available at https://doi.org/doi:10.7278/S50D-G31E-NFW2.

References

Beitler, B., Parry, W. T., & Chan, M. A. (2005). Fingerprints of Fluid Flow: Chemical Diagenetic History of the Jurassic Navajo Sandstone, Southern Utah, U.S.A. *Journal of Sedimentary Research*, *75*(4), 547–561. https://doi.org/10.2110/jsr.2005.045

Bensen, G. D., Ritzwoller, M. H., Barmin, M. P., Levshin, A. L., Lin, F., Moschetti, M. P., et al. (2007). Processing seismic ambient noise data to obtain reliable broad-band surface wave dispersion measurements. *Geophysical Journal International*, *169*(3), 1239–1260. https://doi.org/10.1111/j.1365-246X.2007.03374.x

Biek, R. F., Rowley, P. D., Anderson, J. J., Maldonado, F., Moore, D. W., Hacker, D. B., et al. (2015). Geologic map of the Panguitch 30' x 60' quadrangle, Garfield, Iron and Kane Counties, Utah. Utah Geological Survey Map 270DM, scale 1:62500.

Bieniawski, Z. T. (1978). Determining rock mass deformability: experience from case histories. *International Journal of Rock Mechanics and Mining Sciences And*, *15*(5), 237–247. https://doi.org/10.1016/0148-9062(78)90956-7

Bottelin, P., Lévy, C., Baillet, L., Jongmans, D., & Guéguen, P. (2013). Modal and thermal analysis of les arches unstable rock column (vercors massif, french alps). *Geophysical Journal International*, *194*(2), 849–858. https://doi.org/10.1093/gji/ggt046

Bottelin, P., Jongmans, D., Baillet, L., Lebourg, T., Hantz, D., Lévy, C., et al. (2013). Spectral analysis of prone-to-fall rock compartments using ambient vibrations. *Journal of Environmental and Engineering Geophysics*, *18*(4), 205–217. https://doi.org/10.2113/JEEG18.4.205

Carder, D. S. (1937). Observed Vibrations in Bridges. *Bulletin of the Seismological Society of America*, *27*(4), 267–303.

Chopra, A. K. (2011). *Dynamics of Structure* (4th ed.). Upper Saddle River, NJ: Prentice Hall.

Clinton, J. F., Bradford, S. C., Heaton, T. H., & Favela, J. (2006). The observed wander of the natural frequencies in a structure. *Bulletin of the Seismological Society of America*, *96*(1), 237–257. https://doi.org/10.1785/0120050052

Darbre, G. R., De Smet, C. A. M., & Kraemer, C. (2000). Natural frequencies measured from ambient vibration response of the arch dam of Mauvoisin. *Earthquake Engineering and Structural Dynamics*, *29*(5), 577–586. https://doi.org/10.1002/(SICI)1096-9845(200005)29:5<577::AID-EQE924>3.0.CO;2-P

Doebling, S. W. S., Farrar, C. R. C., Prime, M. B. M., & Shevitz, D. W. D. (1996). Damage identification and health monitoring of structural and mechanical systems from changes in their vibration characteristics: a literature review. *Los Alamos National Laboratory*. https://doi.org/10.2172/249299

Doelling, H. H. (2004). Geologic map of the La Sal 30' x 60' quadrangle, San Juan, Wayne, and Garfield Counties, Utah, and Montrose and San Miguel Counties, Colorado. Utah Geological Survey Map 205, scale 1:100000. https://doi.org/10.34191/M-205

Doelling, H. H., Ross, M. L., Mulvey, W. E., & Creek, M. (2002). Geologic map of the Moab 7.5' quadrangle, Grand County, Utah. Utah Geological Survey Map 181, scale 1:24000.

Dowding, C. H., & Cummings, R. A. (1983). Response of Rock Pinnacles to Blasting Vibrations and Airblasts. *Bulletin of the Association of Engineering Geologists*, *20*(3), 271–281.

Ewins, D. J. (1984). *Modal Testing: Theory and Practice*. New York: John Wiley.

Farrar, C. R., & James III, G. . (1997). System Identification From Ambient Vibration Measurements on a Bridge. *Journal of Sound and Vibration*, *205*(1), 1–18.

Hoek, E., & Diederichs, M. S. (2006). Empirical estimation of rock mass modulus. *International Journal of Rock Mechanics and Mining Sciences*, *43*(2), 203–215. https://doi.org/10.1016/j.ijrmms.2005.06.005

King, K. W., & Demarco, M. J. (2003). Impacts of Construction Vibrations on Rock Pinnacles and Natural Bridges, General Hitchcock Highway, Tucson, Az. In *Proceedings Third International Conference on Applied Geophysics*. Orlando, FL.

Kleinbrod, U., Burjánek, J., & Fäh, D. (2017). On the seismic response of instable rock slopes based on ambient vibration recordings Seismology. *Earth, Planets and Space*, *69*(1). https://doi.org/10.1186/s40623-017-0712-5

Koper, K. D., & Hawley, V. L. (2010). Frequency dependent polarization analysis of ambient seismic noise recorded at a broadband seismometer in the central United States. *Earthquake Science*, *23*(5), 439–447. https://doi.org/10.1007/s11589-010-0743-5

Larose, E., Carrière, S., Voisin, C., Bottelin, P., Baillet, L., Guéguen, P., et al. (2015). Environmental seismology: What can we learn on earth surface processes with ambient noise? *Journal of Applied Geophysics*, *116*, 62–74. https://doi.org/10.1016/j.jappgeo.2015.02.001

Lévy, C., Baillet, L., Jongmans, D., Mourot, P., & Hantz, D. (2010). Dynamic response of the Chamousset rock column (Western Alps, France). *Journal of Geophysical Research: Earth Surface*, *115*(4), 1–13. https://doi.org/10.1029/2009JF001606

Lin, F. C., Li, D., Clayton, R. W., & Hollis, D. (2013). High-resolution 3D shallow crustal structure in Long Beach, California: Application of ambient noise tomography on a dense seismic array. *Geophysics*, *78*(4). https://doi.org/10.1190/geo2012-0453.1

Loope, D. B., Kettler, R. M., & Weber, K. A. (2010). Follow the water: Connecting a CO2reservoir and bleached sandstone to iron-rich concretions in the Navajo Sandstone of south-central Utah, USA. *Geology*, *38*(11), 999–1002. https://doi.org/10.1130/G31213.1

McNamara, D. E., & Buland, R. P. (2004). Ambient Noise Levels in the Continental United States. *Bulletin of the Seismological Society of America*, *94*(4), 1517–1527. https://doi.org/10.1785/012003001

Michel, C., & Gueguen, P. (2010). Time-frequency analysis of small frequency variations in civil engineering structures under weak and strong motions using a reassignment

method. *Structural Health Monitoring*, *9*(2), 159–171. https://doi.org/10.1177/1475921709352146

Moore, J. R., Thorne, M. S., Koper, K. D., Wood, J. R., Goddard, K., Burlacu, R., et al. (2016). Anthropogenic sources stimulate resonance of a natural rock bridge. *Geophysical Research Letters*, *43*(18), 9669–9676. https://doi.org/10.1002/2016GL070088

Moore, J. R., Geimer, P. R., Finnegan, R., & Thorne, M. S. (2018). Use of Seismic Resonance Measurements to Determine the Elastic Modulus of Freestanding Rock Masses. *Rock Mechanics and Rock Engineering*, *51*(12), 3937–3944. https://doi.org/10.1007/s00603-018-1554-6

Park, J., Vernon, F. L., & Lindberg, C. R. (1987). Frequency dependent polarization analysis of high-frequency seismograms. *Journal of Geophysical Research*, *92*(B12), 12664. https://doi.org/10.1029/JB092iB12p12664

Peeters, B., & De Roeck, G. (2001). One-year monitoring of the Z24-bridge: Environmental effectsversus damage events. *Earthquake Engineering and Structural Dynamics*, *30*(2), 149–171. https://doi.org/10.1002/1096-9845(200102)30:2<149::AID-EQE1>3.0.CO;2-Z

Satake, N., Suda, K., Arakawa, T., Sasaki, A., & Tamura, Y. (2003). Damping Evaluation Using Full-Scale Data of Buildings in Japan. *Journal of Structural Engineering*, *129*(4), 470–477. https://doi.org/10.1061/(asce)0733-9445(2003)129:4(470)

Silva, J. M. . (1999). An overview of the fundamentals of modal analysis. In J. M. . Silva & N. M. M. Maia (Eds.), *Modal Analysis and Testing* (pp. 1–34). Dordrecht, Netherlands: Kluwer Academic Publishers.

Starr, A. M., Moore, J. R., & Thorne, M. S. (2015). Ambient resonance of Mesa Arch, Canyonlands National Park, Utah. *Geophysical Research Letters*, *42*(16), 6696–6702. https://doi.org/10.1002/2015GL064917

Ward, K. M., & Lin, F. C. (2017). On the viability of using autonomous three-component nodal geophones to calculate teleseismic ps receiver functions with an application to old faithful, Yellowstone. *Seismological Research Letters*, *88*(5), 1268–1278. https://doi.org/10.1785/0220170051

Welch, P. D. (1967). The Use of Fast Fourier Transform for the Estimation of Power Spectra: A Method Based on Time Averaging Over Short, Modified Periodograms. *IEEE Transactions on Audio and Electroacoustics*. https://doi.org/10.1109/TAU.1967.1161901

Young, W. C., & Budynas, R. G. (2002). Dynamic and Temperature Stresses. In *Roark's Formulas for Stress and Strain* (7th ed., p. 852). New York: Mcgraw-Hill. https://doi.org/10.1016/B978-0-444-41899-9.50020-3

Zadler, B. J., Le Rousseau, J. H. L., Scales, J. A., & Smith, M. L. (2004). Resonant ultrasound spectroscopy: Theory and application. *Geophysical Journal International*, *156*(1), 154–169. https://doi.org/10.1111/j.1365-246X.2004.02093.x

Table 1. Modal analysis results, sorted by total modal misfit.

Site Name	*Site Code*	*Span (m)*	*Formation*	*E (GPa)*	Misfit (%)			Damping Ratio ($\zeta \pm \sigma$ %)
					Total	*Freq.*	*Orient.*	
Moonshine Arch	MOON	21	Navajo	2.4	10	-2	11	2.8 ± 0.2
Arsenic Arch	ARS	2.5	Navajo	0.8	13	-14	21	1.4 ± 0.2
Big Arrowhead Arch	BARH	7	Cedar Mesa	2.7	19	20	35	1.2 ± 0.2*
Moonrise Arch	MRIS	12	Navajo	2.7	21	26	37	1.3 ± 0.2*
Ednah Natural Bridge	EDNA	9.5	Kayenta	3.0	23	6	52	1.4 ± 0.3
Aqueduct Arch	AQUA	24	Wingate	1.8	29	-19	67	1.6 ± 0.2
Landscape Arch	LAND	88.5	Entrada	7.3	29	-5	51	2.7 ± 0.1
Rainbow Bridge	RAB	84	Navajo	4.7	29	37	26	2.4 ± 0.2
Longbow Arch	LNGB	35	Navajo	3.4	31	14	57	1.9 ± 0.2
Rainbow Arch	RAIN	3.5	Entrada	2.0	35	-13	89	1.0 ± 0.2*
Corona Arch	COR	33.5	Navajo	3.5	36	55	54	1.9 ± 0.1
Causeway Arch	CAUS	11	Navajo	1.0	49	32	102	2.5 ± 0.1*
Sunset Arch	SSET	18	Navajo	2.3	49	5	122	1.3 ± 0.1*
Two Bridge	TWBR	9	Claron	5.2	56	-53	104	0.9 ± 0.1*
Owachomo Bridge	OWO	55	Cedar Mesa	8.0	57	31	137	2.6 ± 0.3
Squint Arch	SQNT	12	Navajo	2.1	66	-38	148	1.6 ± 0.3*
Little Bridge Arch	LTBR	11.5	Cutler	3.0	87	57	205	2.7 ± 0.3

Note: * denotes verification via logarithmic decay. Misfit quantifies agreement between predicted and observed modal behavior of each arch using the first three modes, with values approaching zero as agreement improves. Resonant frequency and orientation misfit are the summed percentage differences between predicted and observed values. Total misfit sums absolute frequency and orientation misfit and normalizes to a theoretical poorly-described site with total misfit of 100%, where predicted frequencies and orientations differ from observations by 50% and 90°, respectively.

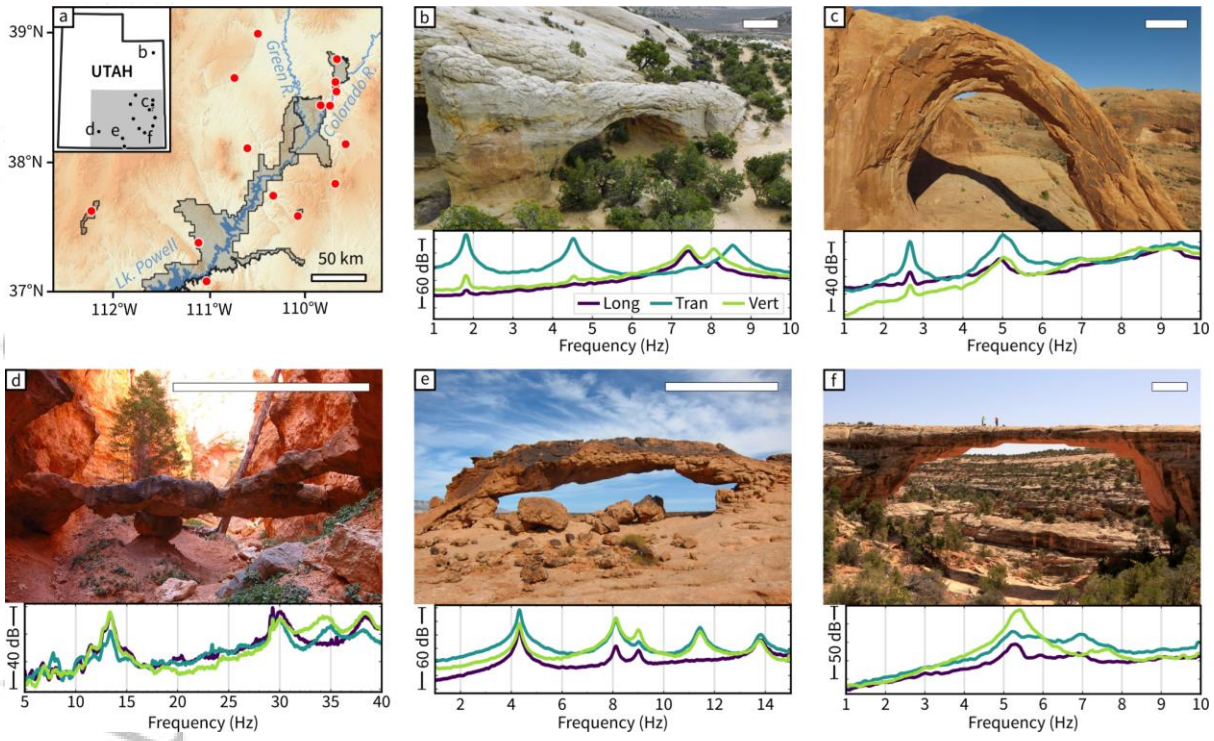

Figure 1. (a) Locations of studied arches within Utah (filled circles). Letters indicate arch locations in following panels. Shaded regions are partnering units of the National Park Service. (b-f) Selected sites – Moonshine Arch, Corona Arch, Two Bridge, Sunset Arch, and Owachomo Bridge – with corresponding three-component power spectral densities. Horizontal channels are rotated to longitudinal and transverse of arch orientation. Relative power is given in decibel units of spectral acceleration, $10\log_{10}$ [m^2/s^4/Hz]. White scale bars in photos are 5 m.

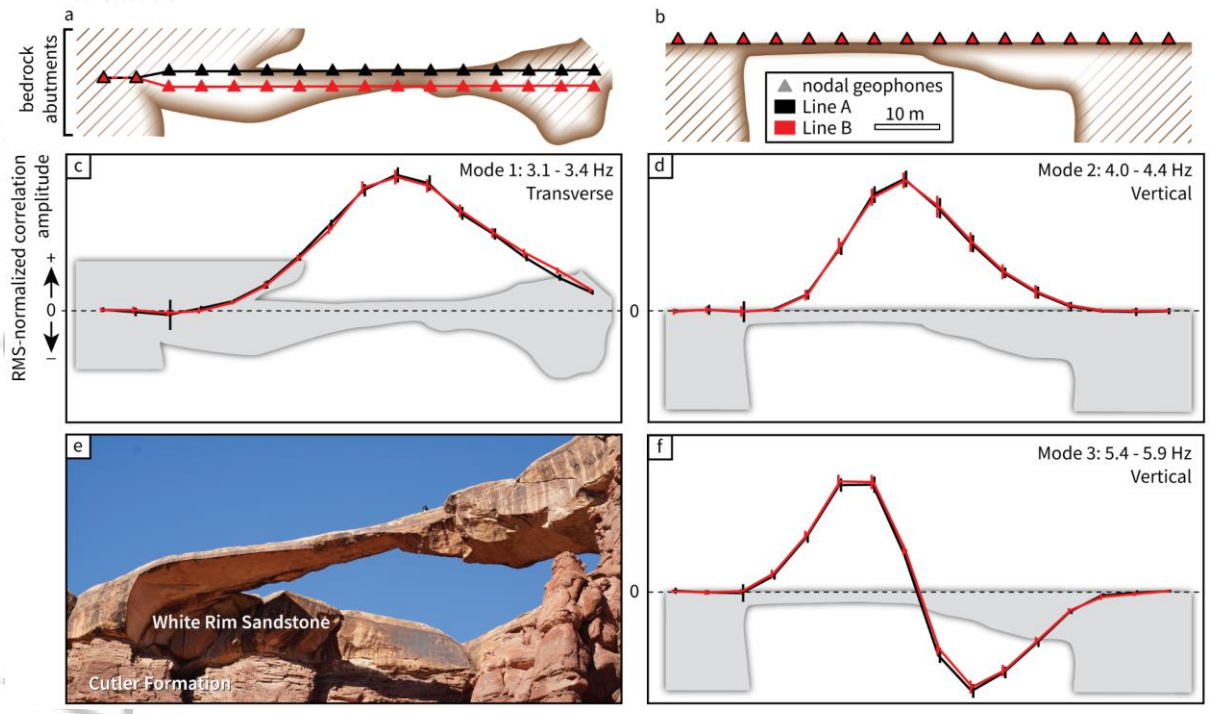

Figure 2. First three mode shapes of Musselman Arch calculated from correlation of a dense geophone array. (a,b) Top and side views show arch geometry, inferred abutment extents, and station locations. (c,d,f) Identified modes on Line A (black) and B (red) using RMS-normalized mean correlation amplitude with ±1 standard deviation bars plotted at each station location. In-phase motion is positive and out-of-phase is negative. (e) Oblique photo of Musselman Arch with geologic units labeled.

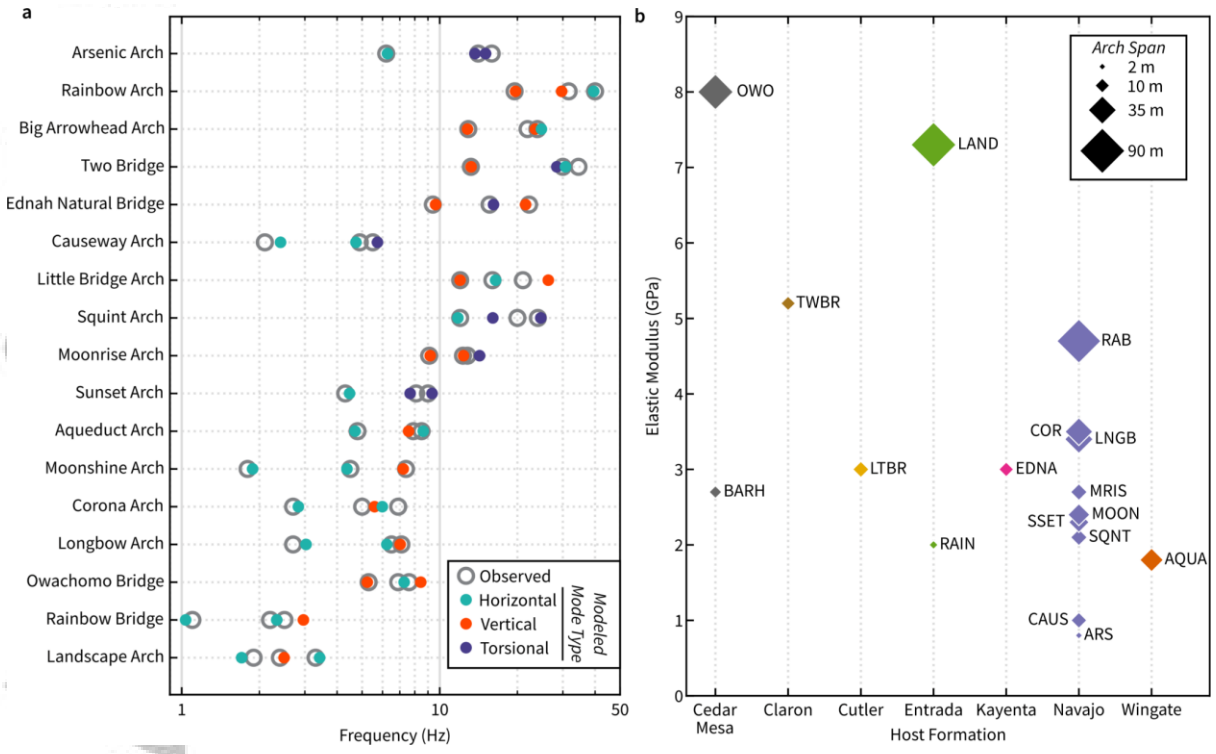

Figure 3. Modal analysis results for 17 arches. (a) Modeled (filled circles) and measured (open) resonant frequencies are plotted on a log scale, with sites sorted by arch span. Color indicates modeled bending mode type. (b) Best-fitting elastic modulus, with color and sorting by host formation, and marker size proportional to arch span. Site codes are given in Table 1.

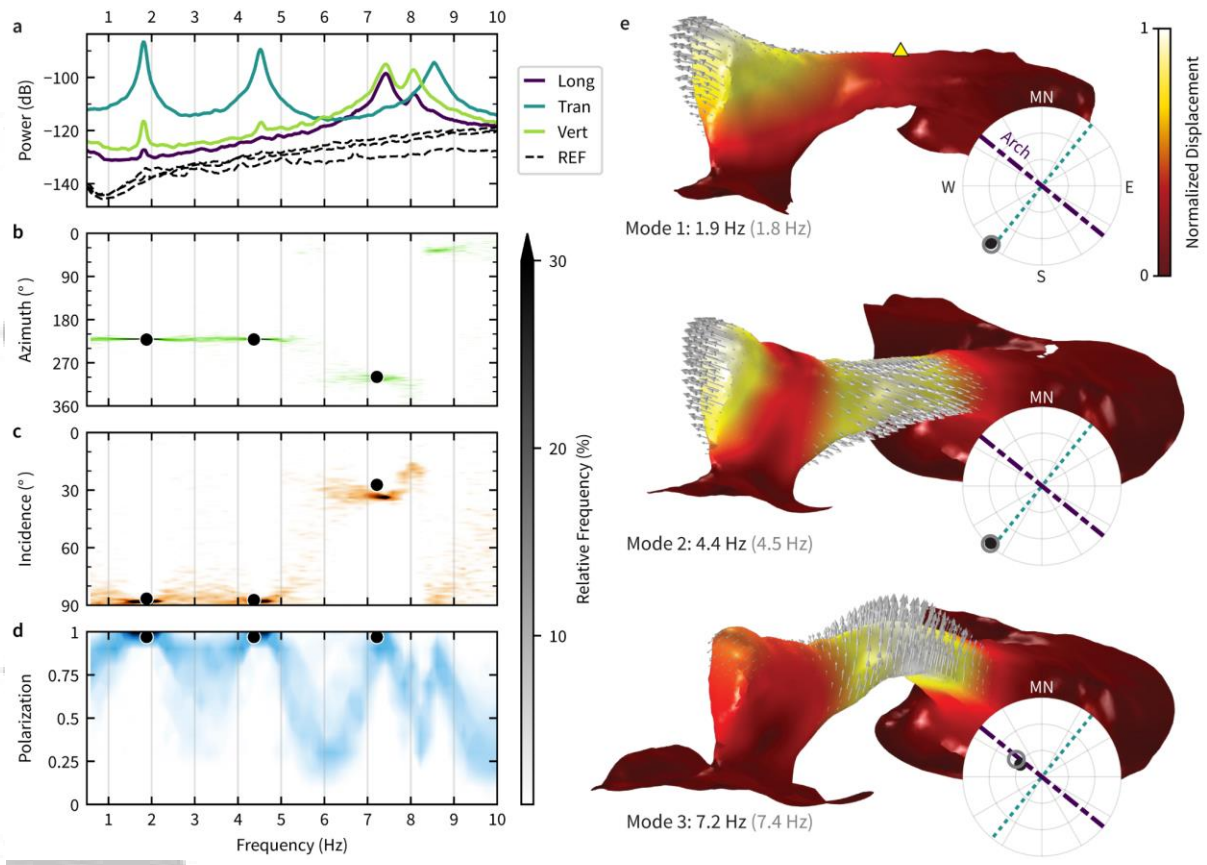

Figure 4. Modal analysis results for Moonshine Arch. (a) One-hour PSD of active (solid) and reference (dashed) channels. Power is given in decibels. (b-d) Probability distributions of polarization azimuth, incidence, and degree of polarization, with modeled results (filled circles). (e) First three modeled mode shapes and frequencies; measured frequencies given in parentheses. Triangle marks the active station location. Relative modal displacement shown by deformation, color map, and arrows. Inset stereo plots compare lower-hemisphere projections of modeled (filled circles) and measured (open) polarization vectors. Dashed lines show longitudinal and transverse arch orientations with respect to magnetic north (MN).